COBEM 2023 27TH INTERNATIONAL CONGRESS OF MECHANICAL ENGENEERING

ABCM Brazilian Society of Mechanical Sciences and Engineering
27th ABCM International Congress of Mechanical Engineering
December 04-08, 2023, Florianópolis-SC, Brazil

COB-2023-0378
An investigation of wave propagation in rotating shafts with attached disks

Gilberto de Sousa Pinheiro Filho
Laís Bitencourt Visnadi
Adriano Todorovic Fabro
Departament of Mechanical Engineering, University of Brasília, Brasília-DF, Brazil
220003122@aluno.unb.br
lais.visnadi@unb.br
fabro@unb.br

Abstract. *Vibration in rotors affects the performance and lifespan of several systems, like gas turbines, oil pumps, and high-speed electrical motors. With an ever-increasing demand for greener and more efficient machinery, the size and speed of rotors also tend to increase, exacerbating the aforementioned problems. Several methods of vibration control have been applied to address these issues, such as precise balancing and high-performance bearings. They are very effective and have been widely applied but have limited performance for the increasingly lighter and higher rotating speed designs of rotating machines. The gyroscopic motion present on rotors generates helical waves combining bending waves of both orthogonal directions. They whirl and vibrate on different frequencies depending on the type of forward or backward excitation. These gyroscopic effects have to be taken into account in the design and vibration control strategies of rotating machines. One promising area of research on this topic is the rotating metamaterials, which can be tuned to affect the specific response to forward or backward excitation in different frequency bands. However, the dynamics of such systems still lack further investigation. This work presents a wave propagation analysis of a rotating system composed of a shaft with attached disks. The investigation is carried out using spectral element and finite element models both assuming a Timoshenko beams model for the shaft and thin disks for the rotors. The wave analysis assumes an infinitely long shaft with periodic attachments and a finite length model assumes bearings at both ends as lumped spring dampers with set stiffness and viscous damping. The focus of the investigation is on the generation of attenuation bands, or band gaps, on the dispersion curves. The case of multiple disks evenly attached to the shaft is investigated. In this case, a band gap is generated, which is expected, since the system resembles a metastructure. In conclusion, it is shown that using a metamaterial approach can be an effective way of controlling vibrations on those systems, but suitable wave behaviour must be considered for the design of the vibration control strategy.*

Keywords: *Wave propagation, Rotordynamics, Metamaterials, Vibration control, Spectral elements*

1. INTRODUCTION

Rotating machines are used in every industry sector. Some, like gas turbines and oil pumps, require machines with ever-increasing capacities and efficiency, which in turn demand higher rotation speeds, intensifying vibrations, and putting machines at elevated risk of failure, which may compromise equipment operation. In any industrial setting, catastrophic failure of a rotating machine causes not only the monetary impact of the loss of said machine but more importantly, may cause serious injuries, deaths, stoppages, and many other physical or financial damages.

Usually, shafts with high rotation speeds, like the ones used in gas turbines, are mounted on hydraulic bearings, this type of bearing has issues concerning wear and fluid-induced instabilities , which limits its vibration control potential, on the upper end of the operational range, as seen in Bently and Hatch'Charles (2003). An innovation that allows increasing speeds in an efficient and clean manner is utilising externally pressurised gas-lubricated bearings like the ones studied in Delgado and Ertas (2019). Another bearing technology being actively developed is magnetic bearings, which allow for passive, semi-active, and active control, as shown in Knospe (2007), an implementation of this type of equipment is shown in Cavalini Junior *et al.* (2013). Although promising solutions, progress in vibration control should not be limited to bearing technology. Alternative solutions, that may better adapt to operational conditions or construction limitations should be researched. One of those is the utilisation of metamaterials, that has been getting traction in the last decades.

The utilisation of meta-structures for vibration control has been extensively explored in the literature, for instance, Hussein *et al.* (2014) and Dalela *et al.* (2022) give detailed overviews of the history of the subject up to the release of the article. The effect of local resonance generates a region on the frequency band where there is wave attenuation on the main structure, also known as a band gap. The design of the locally resonant metamaterial is mainly centred on the tuning of the lowest natural frequencies of the unit cell resonator. The band gap will be formed in this frequency band. In rotating machines, this should be designed such that it is close to the operating frequency range.

Rotating systems have a particular dynamic behaviour related to the gyroscopic effects of the shaft and the elements attached to it. This behaviour can be described as a split of the natural frequencies at rest as the axis starts to rotate. The separation grows as the rotation speed rises. This gyroscopic effect has an influence on the wave propagation behaviour of the structure. If a bare axis is analysed, at rest, the waves propagating on it are planar, when rotation is considered, those waves get a spatial characteristic, becoming helices, which can have right or left-hand chirality, depending on the type of excitation, and each of these can propagate with a forward or backward whirl, which is the rotation of the wave itself, at the natural frequency associated with it. The forward whirl has the same rotation direction as the rotation of the axis, and the backward whirl rotates in the direction opposite to the axis rotation, as described by Chan *et al.* (2005).

Brandão *et al.* (2022) presents a concept of a resonator with a flexible attachment to the axis, that allows for two types of modes of the resonators: translation and rotation. In translation mode, the resonator moves on a plane perpendicular to the rotation axis, like the one shown in Prado and Ritto (2020). This diminishes the importance of the gyroscopic effects on vibration control. In rotation mode, the resonator rotates about an axis perpendicular to the rotation axis. This movement shows strong gyroscopic behaviour. The resonator is illustrated in Figure 1. In this work, it is possible to note the band gap on the desired frequency with both concepts. In the rotational model, the attenuation effect has a particularity, it generates two band gaps related to the forward and backward modes. Each of these interacts only with waves on the same mode, that is, the forward band gap interacts only with the forward modes, likewise, the backward band gap interacts only with the backward modes. This requires careful tuning and may restrict the application of rotational resonators since it's easier to tune the backward band gap.

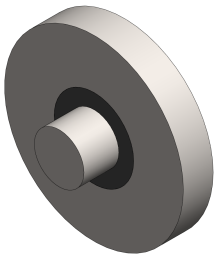

Figure 1. Resonator with flexible attachment to the axis, the black ring is compliant and can be made of rubber of plastic for example. Its material and geometry are the main tuning parameters. Adapted from Brandão *et al.* (2022).

This work aims to further investigate the wave propagation characteristics of a metamaterial implemented on a rotating shaft, focusing on the dispersion behaviour of the resonator rings, and comparing it to the band gap generation capabilities.

2. Methodology

The system in question is a shaft with disks attached to it. Those disks have a flexible connection to the shaft. All the elements used can be modelled as 1D elements, and are very well documented, with analytical shape functions like the ones presented in Lee (2009). Because of that, the spectral element method (SEM) is a convenient approach, and it will be the main method used in this work since it does not require mesh refinement and generally gives smaller matrices, although full and complex, and typically requires less computational time if compared to the finite element method (FEM). But there will be a section comparing the results obtained by using SEM to the results using FEM since the latter is widely available in various packages. The implementation used as comparison is the one used in ROSS, which is detailed in Timbó *et al.* (2020).

2.1 Shaft model

The geometrical parameters, like length and diameter, of the shaft and its elements and stiffness values of the bearings were defined based on the work of Cavalini Junior *et al.* (2013). The elements present in the model are the shaft, which is 660 mm long from bearing to bearing (the tips are not taken into account) and 17 mm in diameter, and the inertia disk, which with a diameter of 200 mm and a thickness of 20 mm, it is rigidly attached to the shaft, the resonators, which have 50 mm diameter and 10 mm thickness, and the bearings, which have fixed stiffness coefficients shown in table 1. Figure 2 shows a CAD model of the assembly.

This model was discretized using Timoshenko beams for the shaft elements, thin disk elements with rigid attachments for the inertia disk, and thin disk elements with rigid or flexible attachments for the resonator rings. The thin disk element does not add new degrees of freedom between shaft elements, this simplifies the matrix assembly while still giving accurate results, as shown in Lee (2009). The resonator rings with flexible attachment do add degrees of freedom but they do not space out the beam elements, only adding a node on top of the existing connection. Figure 3 shows the rotor, with

Table 1. Bearing stiffness, obtained from Cavalini Junior *et al.* (2013).

	K_{yy}	K_{zz}	C_{yy}	C_{zz}
Left Bearing	8.551e5	1.198e6	7.452	33.679
Right Bearing	5.202e7	7.023e8	25.6	91

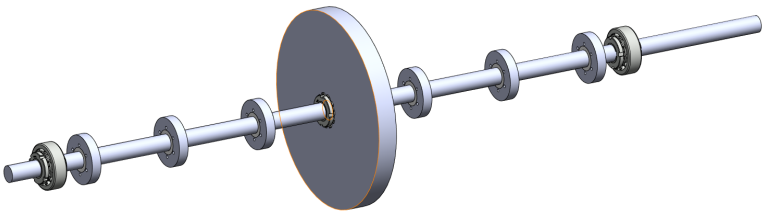

Figure 2. CAD model of the shaft in question, showing the two bearings considered, the inertia disk and 6 resonators

6 resonators, spectral element discretization. The spectral element method does not require mesh refinement, and new elements only need to be added on discontinuities, such as the rings. Still, it can be seen that between two rings there are two shaft elements, which are not for mesh refinement, but to facilitate the automation of the shaft building in software.

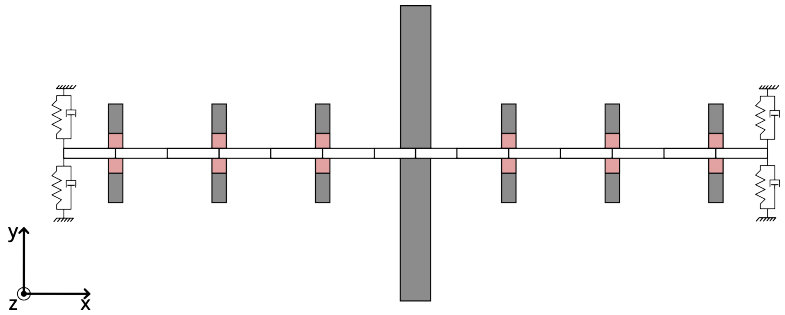

Figure 3. Model discretization, the bearings are represented as stiffness on each end of the shaft, in this image, 6 resonators cells are represented along with the inertia disk cell, the cell attachment is represented by the pink squares, and may be rigid, like a steel bushing, or flexible, like a rubber ring.

The implementation of spectral elements was based on the formulation present in Lee (2009) and the code was written in Python. The Timoshenko beam element has 12 degrees of freedom, 6 at each node, and the thin disk element with rigid attachment has 6 degrees of freedom. The resonator disk element also has 6 degrees of freedom but they are independent of the node they are attached to, having the motion transmitted to and from them via stiffness and damping matrices.

2.2 Spectral Element Modeling

In this section, the spectral element formulation is briefly presented, for more detailed development of the elements refer to Lee (2009). The spectral element equation for the Timoshenko beam is condensed to a two-noded element as

$$\mathbf{S^S}(\omega)\boldsymbol{d^S}(\omega) = \boldsymbol{f^S}(\omega), \tag{1}$$

where $\mathbf{S^S}$ is the spectral element matrix, $\boldsymbol{d^S}$ is the degrees of freedom vector, $\boldsymbol{f^S}$ is forcing vector and ω is the angular frequency, which is omitted in following equation for simplification of notation unless otherwise required. It can be rewritten in a block-matrix form as

$$\begin{bmatrix} \mathbf{S^S_{11}} & \mathbf{S^S_{12}} \\ \mathbf{S^S_{21}} & \mathbf{S^S_{22}} \end{bmatrix} \begin{Bmatrix} \boldsymbol{d}_1^S \\ \boldsymbol{d}_2^S \end{Bmatrix} = \begin{Bmatrix} \boldsymbol{f}_1^S \\ \boldsymbol{f}_2^S \end{Bmatrix}, \tag{2}$$

where the suffix 1 relates to the left side of the beam and 2 to the right side. This matrix is not symmetric due to the gyroscopic effects. Expanding the matrices $\mathbf{S^S_{ij}}$ and vectors $\boldsymbol{d}_j^S$ and $\boldsymbol{f}_j^S$:

$$\mathbf{S_{ij}^{S}} = \begin{bmatrix} S_{L_{ij}} & 0 & \mathbf{0} \\ 0 & S_{T_{ij}} & \mathbf{0} \\ \mathbf{0} & \mathbf{0} & \mathbf{S}_{B_{ij}} \end{bmatrix}, \quad (i,j = 1,2) \tag{3}$$

where $S_{L_{ij}}$ is related to the longitudinal motion along the shaft (x), $S_{T_{ij}}$ to the torsion of the axis, and $\mathbf{S}_{B_{ij}}$ is related to the bending motion of the shaft around the directions y and z, thus a 4 by 4 non-symmetric matrix, the terms on the secondary diagonal appear due to gyroscopic effects.

For the attached disks, two types of coupling were modelled, the inertia disk is rigidly attached, and the resonators are flexibly attached. The elemental matrices are given in terms of mass, gyroscopic, stiffness and damping matrices. The mass matrix of the rotor and resonator rings is given as

$$\mathbf{M_r} = \begin{bmatrix} M_D & 0 & 0 & 0 & 0 & 0 \\ 0 & J_D & 0 & 0 & 0 & 0 \\ 0 & 0 & M_D & 0 & 0 & 0 \\ 0 & 0 & 0 & I_D & 0 & 0 \\ 0 & 0 & 0 & 0 & M_D & 0 \\ 0 & 0 & 0 & 0 & 0 & I_D \end{bmatrix}, \tag{4}$$

where M_D is the mass of the disk, J_D is the moment of inertia in x and I_D is the moment of inertia in the directions y and z. The gyroscopic matrix is given as

$$\mathbf{G_r} = \begin{bmatrix} 0 & 0 & 0 & 0 & 0 & 0 \\ 0 & 0 & 0 & 0 & 0 & 0 \\ 0 & 0 & 0 & 0 & 0 & 0 \\ 0 & 0 & 0 & 0 & 0 & \Omega J_D \\ 0 & 0 & 0 & 0 & 0 & 0 \\ 0 & 0 & 0 & -\Omega J_D & 0 & 0 \end{bmatrix}. \tag{5}$$

The gyroscopic matrix couples the bending motion of y and z and is proportional to the rotation of the shaft Ω and J_D, the latter is the main tuning parameter if the more or less gyroscopic effect is desired, and can be adjusted by modifying resonator mass or spatial distribution of this mass.

The coupling stiffness matrix is shown in equation 6 and is only used for the flexible attachment.

$$\mathbf{K_r} = \begin{bmatrix} k_a & 0 & 0 & 0 & 0 & 0 \\ 0 & k_{tt} & 0 & 0 & 0 & 0 \\ 0 & 0 & k_t & 0 & 0 & 0 \\ 0 & 0 & 0 & k_r & 0 & 0 \\ 0 & 0 & 0 & 0 & k_t & 0 \\ 0 & 0 & 0 & 0 & 0 & k_r \end{bmatrix} \tag{6}$$

k_a is coupling stiffness in the axial direction (x), k_{tt} is the torsional stiffness, k_t is the translational stiffness, and k_r is the rotational stiffness (rotation around the y and z axes). The damping is considered proportional to the stiffness matrix and is shown in equation 7.

$$\mathbf{C_r} = c_p \mathbf{K_r} \tag{7}$$

The dynamic stiffness matrices for the rigidly attached disks is

$$\mathbf{D} = \begin{bmatrix} \mathbf{S}_{11}^1 & \mathbf{S}_{12}^1 & \mathbf{0} \\ \mathbf{S}_{21}^1 & \mathbf{S}_{22}^1 - \omega^2 \mathbf{M_r} - i\omega \mathbf{G_r} + \mathbf{S}_{11}^2 & \mathbf{S}_{12}^2 \\ \mathbf{0} & \mathbf{S}_{21}^2 & \mathbf{S}_{22}^2 \end{bmatrix}. \tag{8}$$

For the flexibly attached disks, the dynamic stiffness matrix is given as

$$\mathbf{D} = \begin{bmatrix} \mathbf{S}_{11}^1 & \mathbf{S}_{12}^1 & \mathbf{0} & \mathbf{0} \\ \mathbf{S}_{21}^1 & \mathbf{S}_{22}^1 + \mathbf{S}_{11}^2 + \mathbf{K_r} - i\omega \mathbf{C_r} & \mathbf{S}_{12}^2 & -\mathbf{K_r} + i\omega \mathbf{C_r} \\ \mathbf{0} & \mathbf{S}_{21}^2 & \mathbf{S}_{22}^2 & \mathbf{0} \\ \mathbf{0} & -\mathbf{K_r} + i\omega \mathbf{C_r} & \mathbf{0} & -\omega^2 \mathbf{M_r} - i\omega(\mathbf{G_r} + \mathbf{C_r}) + \mathbf{K_r} \end{bmatrix}, \tag{9}$$

where the superscript indicates from what element those degrees of freedom are, 1 for the left beam and 2 for the right.

It is clear that the flexibly attached resonator adds degrees of freedom to the model, and by building the matrix this way, special care must be taken in the following steps to organise the internal and external degrees of freedom since the degrees of freedom related to the resonator are internal.

2.3 Wave analysis

The wave analysis is performed on the unit cell only. The dynamic matrix obtained previously is reorganised in internal and external DOFs, i.e.,

$$\mathbf{D} = \begin{bmatrix} \mathbf{D}_{LL} & \mathbf{D}_{LI} & \mathbf{D}_{LR} \\ \mathbf{D}_{IL} & \mathbf{D}_{II} & \mathbf{D}_{IR} \\ \mathbf{D}_{RL} & \mathbf{D}_{RI} & \mathbf{D}_{RR} \end{bmatrix}, \tag{10}$$

then a condensation is performed, which yields

$$\mathbf{D}^* = \begin{bmatrix} \mathbf{D}_{LL} - \mathbf{D}_{LI}\mathbf{D}_{II}^{-1}\mathbf{D}_{IL} & \mathbf{D}_{LR} - \mathbf{D}_{LI}\mathbf{D}_{II}^{-1}\mathbf{D}_{IR} \\ \mathbf{D}_{RL} - \mathbf{D}_{RI}\mathbf{D}_{II}^{-1}\mathbf{D}_{IL} & \mathbf{D}_{RR} - \mathbf{D}_{RI}\mathbf{D}_{II}^{-1}\mathbf{D}_{IR} \end{bmatrix}, \tag{11}$$

and it is rewritten as

$$\mathbf{D}^* = \begin{bmatrix} \mathbf{D}_{LL}^* & \mathbf{D}_{LI}^* \\ \mathbf{D}_{IL}^* & \mathbf{D}_{II}^* \end{bmatrix}. \tag{12}$$

In the framework of a periodic structure, the dynamic stiffness matrix can be rewritten as a transfer matrix, that transmits the force and displacement information from one end of the cell to the other, given as

$$\mathbf{T} = \begin{bmatrix} -\mathbf{D}_{LR}^{-1}\mathbf{D}_{LL} & \mathbf{D}_{LR}^{-1} \\ -\mathbf{D}_{RL} + \mathbf{D}_{RR}\mathbf{D}_{LR}^{-1}\mathbf{D}_{LL} & -\mathbf{D}_{RR}\mathbf{D}_{LR}^{-1} \end{bmatrix} \tag{13}$$

Under the Floquet-Bloch assumption, solving an eigenvalue problem with that matrix yields the wavenumbers for each frequency, such that a dispersion diagram can be found for each mode.

2.4 Unit cells

The unit cell model is composed of two shaft elements and a resonator ring with flexible coupling between them, this exploits the attenuation band generated via local resonance.

2.5 Analysis procedure

To establish a baseline and a target frequency to tune the resonators, the shaft with only the inertia disk is simulated and its first bending natural frequency is used as the tuning parameter. The aim is to attenuate vibrations around it. It will later be shown that this implementation of spectral elements does not deal well with low rotation speeds and frequencies, and short lengths. Thus, the rotation speed of the shaft is fixed at 1000 Hz in all analyses, which is non-realistic.

Subsequently, the wave propagation behaviour of the unit cell is investigated. The aim of this step is to identify features on the dispersion diagram that indicate the formation of a band gap or regions of significant frequency attenuation. It is important to highlight the tuning procedure of the resonators. The stiffness values are calculated directly from the target resonance frequency given a corresponding inertia element, in this case, only the translational vibration is of interest, its stiffness will be set so the resonance is on 25 Hz, and the other modes of vibration of the resonator are tuned so that they are far from the lowest resonance frequency, in this case, 100 Hz.

A Python script is used to build the shaft model since the inertia disk is in the centre of the analysed region. The unit cells will be added in pairs. Due to limitations on the size of the shaft and the chosen unit cell size, the maximum number of cells is 6. So, three simulation cases will be performed, with 2, 4 and 6 resonators. The frequency responses compared to the response of the shaft without resonators to investigate the performance of the solutions, the main parameter to evaluate the advantage of adding more resonators will be the widening in the attenuation band. Additionally, this effect must be compared with the added mass to the system.

3. Results

In this section, the numerical results are presented in terms of the forced response from a point harmonic force and in terms of the dispersion diagram, i.e., the wavenumber as a function of frequency for each wave mode. First, the shaft with only the inertia disk was analysed. As stated before, its first natural frequency was calculated at 25.3 Hz and the target frequency for the tuning was chosen as 25 Hz.

3.1 Unit cell wave propagation analysis using SEM

Figure 4 shows the dispersion curves obtained with the undamped flexible attachment. The wave behaviour of this unit cell is complex to analyse since it presents a typical dispersion curve of a locally resonant metamaterial in addition to a veering at low frequencies Mace and Manconi (2012). But it already shows local resonance behaviour, as can be seen in the peak of imaginary value at the calibration frequency.

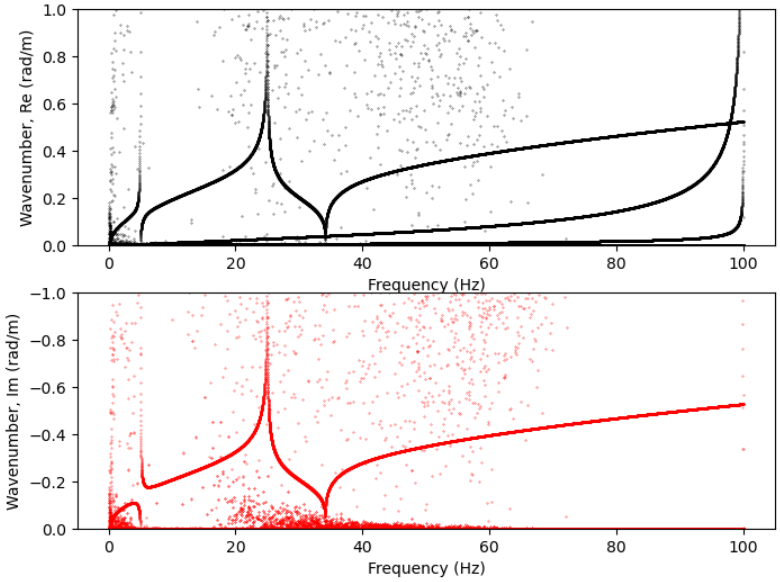

Figure 4. The real (upper) and the imaginary part (lower) of the dispersion diagram for the disk with 50 mm diameter and 10 mm thickness with flexible attachment and no damping.

Subsequently, damping was added in the unit cell model at the connection between the disk and the shaft. The wave behaviour becomes more complex, as can be seen in Figure 5, showing interactions that were not clear in the previous analysis, like coupling between two types of waves at the band gap region, presumably both flexural. Figure 6 shows a detailed view of the region around the design frequency, it can be seen that one of the waves always has a complex component, while the other only becomes complex near the design frequency, and in the real part of the graph there's a peak at the design frequency, indicating attenuation behaviour.

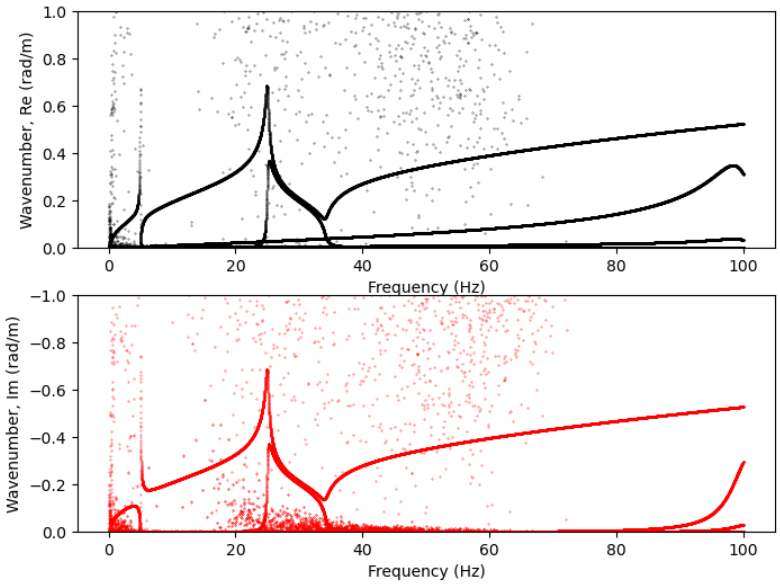

Figure 5. The real (upper) and the imaginary part (lower) of the dispersion diagram for the disk with 50 mm diameter and 10 mm thickness with flexible attachment to the shaft.

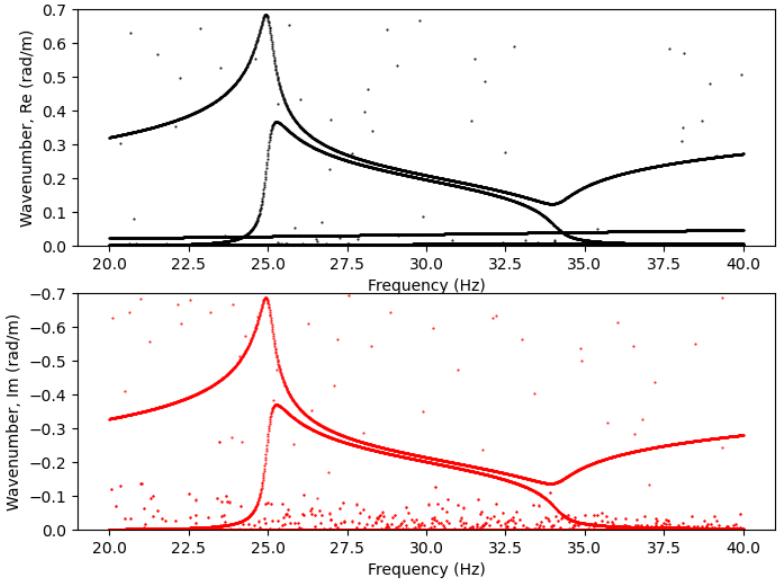

Figure 6. Detail zoom of the dispersion diagram shown in figure 5.

A number of numerical artefacts can be seen in the figures aforementioned. This occurs mostly at low frequencies in this case, but also at and low rotation speeds which are not presented here. This was the main reason why the rotor rotation chosen at 1000 Hz. The cause of this is ill-conditioning of the dynamic stiffness matrices, which have components with very small and very large values, this makes those matrices very susceptible to rounding errors, even when utilising double precision floating numbers, and since the solution requires several inversions, those problems are intensified. This issue is not directly addressed in this work, but the numerical conditioning can be greatly improved by using a regularisation approach (Ribeiro et al., 2023).

3.2 Unit cell wave propagation analysis using FEM

In this section, a finite element analysis will be performed as a means of method comparison and to try and solve the numerical artefacts problem.

Image 7 show the dispersion curves for the unit cell without damping. It can be seen that the graph has fewer elements than the with obtained with SEM, that's because the FEM implementation used has only 4 degrees of freedom. The wave behaviour around the target frequency is equal to the one observed in the SEM analysis but differs on other frequency bands, further investigations must be performed to better access this behaviour.

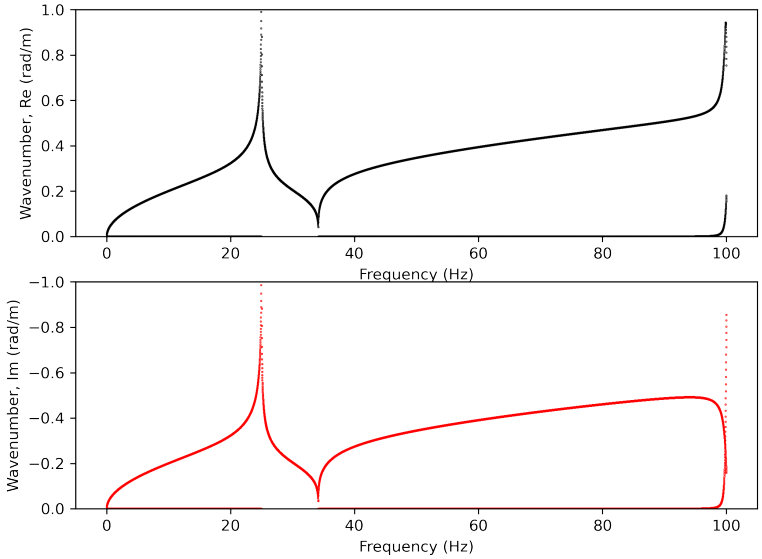

Figure 7. The real (upper) and the imaginary part (lower) of the dispersion diagram for the disk with 50 mm diameter and 10 mm thickness with flexible attachment and no damping.

An analysis with damping was performed, but the results showed little difference compared to the undamped case, as seen in figure 8, not showing the complex interactions observed in the SEM model. This may be due to the lower number of degrees of freedom (the FEM model only uses 4 degrees of freedom, disregarding axial and torsional modes), which neglects the interactions between the different types of waves or may be caused by a different damping model.

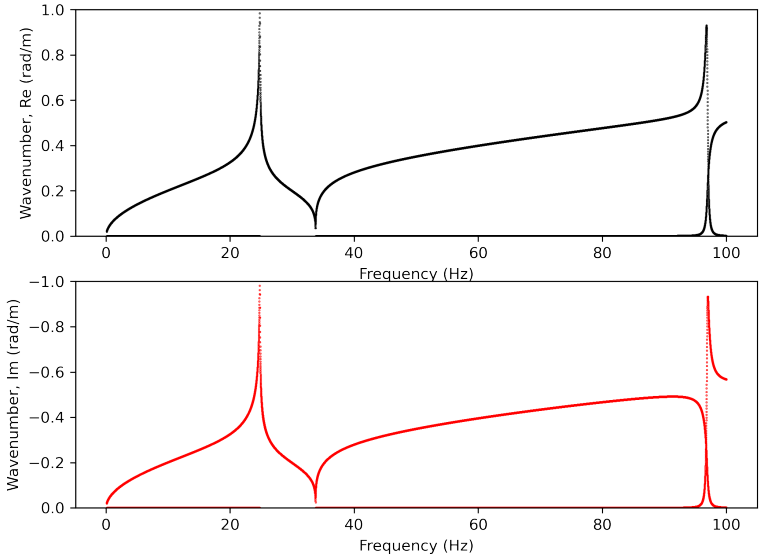

Figure 8. The real (upper) and the imaginary part (lower) of the dispersion diagram for the disk with 50 mm diameter and 10 mm thickness with flexible attachment with proportional damping.

Those results predict quite reliably the band gap formation region and are numerically stable even at low rotation

speeds, which shows that steps must be taken towards better conditioning of the SEM matrices.

3.3 Frequency response analysis

Figure 9 presents the frequency function to a point harmonic force at one of the sides of the shaft with no resonators, 2 resonators, 4 resonators and 6 resonators. It can be seen that there is an attenuation at the target frequency, as predicted in the dispersion curve. Moreover, it is shown that by increasing the number of resonators there is an increase in the attenuation band. However, there is also an increase in the total added mass. It can be noticed that rising from 4 to 6 resonators shows little improvement when compared to the increase from 2 to 4, especially if added mass is taken into account.

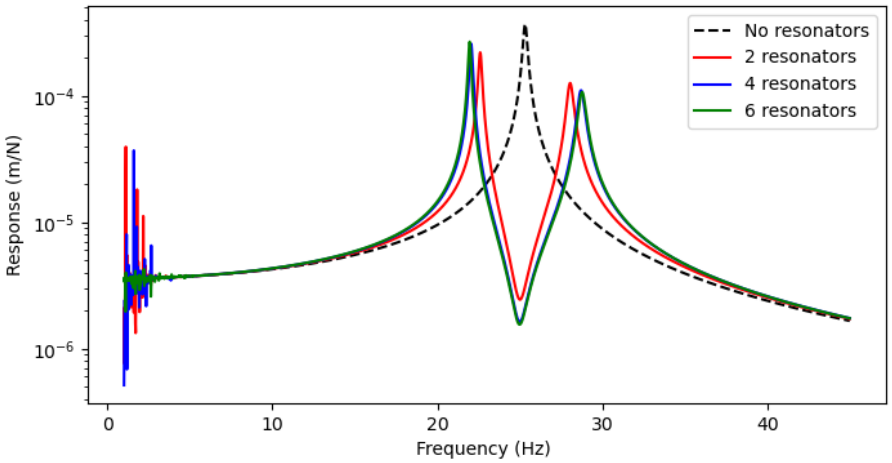

Figure 9. Frequency response functions of the shaft without resonators and with 2, 4 and 6 resonators.

4. Conclusions

To mitigate vibration on rotating machines, a metamaterial is proposed, the resonator presented has a flexible attachment to the shaft. This type of mounting system takes advantage of the local resonance effect, which creates a band gap. To better understand the attenuation behaviour of this metamaterial, a wave propagation study is conducted, initially, using SEM. The results obtained are very promising, clearly showing an attenuation region around the desired frequency range, indicating that this type of vibration control method is viable, a system analysis is performed varying the number of resonators, this shows that there's an optimal number of resonators, further addition of disks has little impact on attenuation band compared to the impact of added weight. The main problem with this approach is that the dispersion curves show heavy numerical artifacting, especially at low frequencies, the main reason for this is the ill-conditioned matrices generated by the SEM algorithm used, which after several inversion operations, give several points with wrong results.

To address the numerical artifacting problem, and to have a basis of comparison for the SEM analysis, a wave FEM analysis was also performed in the unit cell. This analysis was performed in ROSS, an open-source software specialized in rotordynamics. Having much better conditioned matrices, the results obtained were numerically clean, but this came with limitations, the main one is that ROSS works mainly with 4 degrees of freedom (the disks with flexible attachments are not implemented in 6 DOF), and for larger systems, it may require mesh refinement, which will slow down significantly the analysis.

For those reasons, it is important to solve the conditioning problem found in the SEM implementation. There are several methods of pre-conditioning that may solve the issue, like the generalized minimal residual (GMRES) method, or using ridge regression to perform matrix inversions. It is also important to compare the performance of the proposed metamaterial with other solutions, like dynamic absorbers and active bearings. The tuning method must be revised to account for practical limitations on the design of resonators, which may not permit a clear isolation of one type of resonance frequency. After those challenges are overcome, experiments should be performed to validate the vibration control characteristics.

5. ACKNOWLEDGEMENTS

The authors are grateful to the Brazilian National Council of Research (CNPq - Brazil) and the Federal District Foundation for Research Support (FAPDF -Brazil) for the financial support, and to the Pos-Graduation Program in Mechanical Sciences of the University of Brasilia (UnB).

6. REFERENCES

Bently, D.E. and Hatch'Charles, T., 2003. "Fundamentals of rotating machinery diagnostics". *Mechanical Engineering-CIME*, Vol. 125, No. 12, pp. 53–54.

Brandão, A.A., de Paula, A.S. and Fabro, A.T., 2022. "Rainbow gyroscopic disk metastructures for broadband vibration attenuation in rotors". *Journal of Sound and Vibration*, Vol. 532, p. 116982.

Cavalini Junior, A.A. *et al.*, 2013. "Detecção e identificação de trincas transversais incipientes em eixos horizontais flexíveis de máquinas rotativas".

Chan, K., Stephen, N. and Reid, S., 2005. "Helical structure of the waves propagating in a spinning timoshenko beam". *Proceedings of the Royal Society A: Mathematical, Physical and Engineering Sciences*, Vol. 461, No. 2064, pp. 3913–3934.

Dalela, S., Balaji, P. and Jena, D., 2022. "A review on application of mechanical metamaterials for vibration control". *Mechanics of advanced materials and structures*, Vol. 29, No. 22, pp. 3237–3262.

Delgado, A. and Ertas, B., 2019. "Dynamic characterization of a novel externally pressurized compliantly damped gas-lubricated bearing with hermetically sealed squeeze film damper modules". *Journal of Engineering for Gas Turbines and Power*, Vol. 141, No. 2.

Hussein, M.I., Leamy, M.J. and Ruzzene, M., 2014. "Dynamics of phononic materials and structures: Historical origins, recent progress, and future outlook". *Applied Mechanics Reviews*, Vol. 66, No. 4.

Knospe, C.R., 2007. "Active magnetic bearings for machining applications". *Control Engineering Practice*, Vol. 15, No. 3, pp. 307–313.

Lee, U., 2009. *Spectral element method in structural dynamics*. John Wiley & Sons.

Mace, B.R. and Manconi, E., 2012. "Wave motion and dispersion phenomena: Veering, locking and strong coupling effects". *The Journal of the Acoustical Society of America*, Vol. 131, pp. 1015–1028. ISSN 0001-4966. doi: 10.1121/1.3672647. URL `https://asa.scitation.org/doi/10.1121/1.3672647`.

Prado, L. and Ritto, T., 2020. "Vibration reduction of a rotating machine using resonator rings". *Mechanics Research Communications*, Vol. 107, p. 103533.

Timbó, R., Martins, R., Bachmann, G., Rangel, F., Mota, J., Valério, J. and Ritto, T.G., 2020. "Ross - rotordynamic open source software". *Journal of Open Source Software*, Vol. 5, No. 48, p. 2120. doi:10.21105/joss.02120. URL `https://doi.org/10.21105/joss.02120`.

7. RESPONSIBILITY NOTICE

The following text, properly adapted to the number of authors, must be included in the last section of the paper:
The author are solely responsible for the printed material included in this paper.